SAND2021-2340C

Fracture Formation in Layered Synthetic Rocks with Oriented Mineral Fabric under Mixed Mode I and II Loading Conditions

Liyang Jiang
Department of Physics and Astronomy, Purdue University, West Lafayette, IN,USA
Hongkyu Yoon
Geomechanics Department, Sandia National Laboratories, Albuquerque, NM,USA
Antonio Bobet
Lyles School of Civil Engineering, Purdue University, West Lafayette, IN,USA
Laura J. Pyrak-Nolte
Department of Physics and Astronomy, Purdue University, West Lafayette, IN,USA
Lyles School of Civil Engineering, Purdue University, West Lafayette, IN,USA
Department of Earth and Atmospheric Sciences, Purdue University, West Lafayette, IN,USA

ABSTRACT: Anisotropy in the mechanical properties of rock is often attributed to bedding and mineral texture. Here, we use 3D printed synthetic rock to show that, in addition to bedding layers, mineral fabric orientation governs sample strength, surface roughness and fracture path under mixed mode I and II three point bending tests (3PB). Arrester (horizontal layering) and short traverse (vertical layering) samples were printed with different notch locations to compare pure mode I induced fractures to mixed mode I and II fracturing. For a given sample type, the location of the notch affected the amount of mode II loading, and thus affected the peak failure load and fracture path. When notches were printed at the same location, crack propagation, peak failure load and fracture surface roughness were found to depend on both the layer and mineral fabric orientations. The uniqueness of the induced fracture path and roughness is a potential method for the assessment of the orientation and relative bonding strengths of minerals in a rock. With this information, we will be able to predict isotropic or anisotropic flow rates through fractures which is vital to induced fracturing, geothermal energy production and CO_2 sequestration.

1. INTRODUCTION

The layers of sedimentary rocks arise from depositional, compaction and diagenetic processes. Within a layer, preferred mineral orientation caused by interlocking crystals, foliations, or fragments may exist. Past research has shown that layers or preferred mineral orientations are known to affect the mechanical properties of rock leading to direction dependent or anisotropic elastic moduli (Jones and Wang,1981; Vernik and Nur, 1992; Hornby et al., 1994; Sayers, 1994, 2005; Wenk et al., 2007).

Our previous work (Jiang et al., 2019; Jiang et al., 2020) examined the role of mineral fabric orientation in layered rock on tensile fracture formation. For Mode I failure induced through three point bending (3PB) experiments, tensile fracture toughness and roughness were controlled by the relative orientation between the layering and the in-plane mineral fabric.

For anisotropic rock, much research has focused on fracturing behavior for mode I loading conditions because mode I loading occurs the most often and produces the most damage (Nejati et al., 2020). In this work, we present results from 3PB testing with mixed Mode I and II loading of anisotropic synthetic rock by moving the notch on the samples away from the center of the sample (Figure 1).

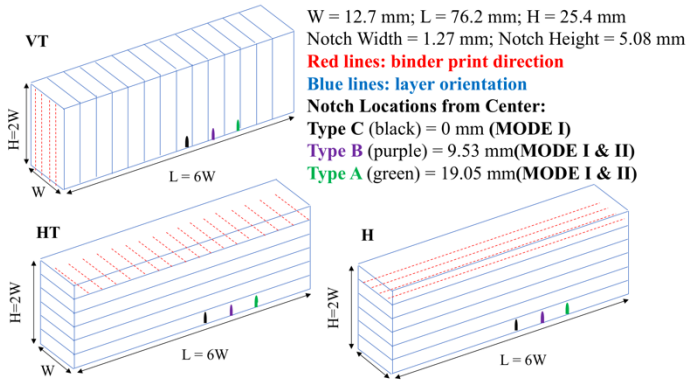

Fig. 1. Sketch of 3D printed anisotropic gypsum samples with different notch locations. VT is the short traverse sample with the mineral fabric orientation shown in red and the layering

Sandia National Laboratories is a multimission laboratory managed and operated by National Technology & Engineering Solutions of Sandia, LLC, a wholly owned subsidiary of Honeywell International Inc., for the U.S. Department of Energy's National Nuclear Security Administration under contract DE-NA0003525.

direction in blue. HT and H are both arrester samples but with different mineral fabric orientations.

For three different sample types with three different notch locations (Figure 1), measurements were performed to determine if the failure load, fracture path, and surface roughness differ significantly when anisotropic rock samples fracture from both tensile and shear loading, as compared to pure tensile failure (mode I only).

2. EXPERIMENTAL APPROACH

2.1. 3D printing Synthetic Rock

Additive manufacturing is a sample fabrication approach that enables the production of synthetic rock samples with repeatable dimensions and material properties for model verification. In this study, layered rock samples with preferred mineral fabric orientation were created using a 3D printing process (ProJet CJP 360 printer). Layers of calcium sulfate hemi-hydrate (0.1 mm thick bassanite powders) were bonded with a proprietary water-based binder (ProJet X60 VisiJet PXL) that produced gypsum as a reaction product (Figure 2). The orientation of the mineral fabric was controlled by the direction of the application of the binder (red arrow in Figure 2b). When one layer of bassanite is deposited on top of a previous layer (Figure 2a), the binder causes gypsum crystals to form a bond between bassanite layers. An oriented mineral fabric arises because the gypsum forms stronger bonds between gypsum crystals than between the gypsum crystals and bassanite powder.

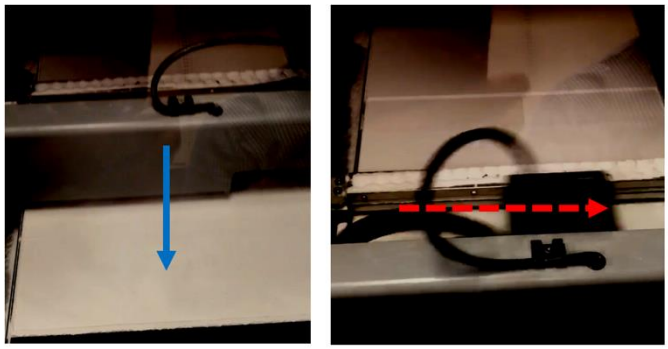

a) Deposition of 0.1 mm thick layer of bassanite powder ($2CaSO_4 \cdot H_2O$) on printing area

b) Spreading of water-based binder in the direction of the red arrow

Fig. 2. Depiction of 3D printing process of gypsum samples: (a) deposition of the bassanite layers; (b) direction of the application of the binder (red arrow).

2.2. Three Point Bending (3PB) Tests

Samples with different orientations of bassanite layers relative to gypsum mineral fabric were 3D printed to examine the effect of fabric direction relative to the bedding layer direction on crack growth under mixed mode loading conditions, and on the geometric properties of the induced fractures. 3D printed samples have been shown to represent natural rocks based on their physical properties (Kong et al., 2018). The dimensions of the sample were 25.4 x 76.2 x 12.7 mm. Figure 1 shows a sketch of the samples with the layer orientation given by the blue lines and the orientation of the mineral fabric given by the red lines. Here the samples are referred to as arrester (H & HT) and short traverse (VT). In addition to the orientation of the bedding layers and mineral fabric, three different notch locations were tested to compare pure Mode I induced fractures with Mixed Mode I & II induced fractures. The notch was located at either 0 (center of the specimen), 9.53 mm, or 19.05 mm from the center (Figure 1), with the name of the samples given by type C, B, or A, respectively.

Tensile and shear fractures (Mode I and II) were induced in samples using a 3PB test setup as shown in Figure 3. A rod (4.76 mm in radius, 19.05 mm in length) was placed on the top surface at the center of the sample and two rods (same sizes) were placed symmetrically on the bottom surface at a distance of 10% of the sample length (7.6 mm from the ends of the sample). Load was applied to a sample using an ELE International Soil Testing load frame with an OMEGA 1112 N capacity S-shaped load cell. The loading rate was 0.03 mm/min. Load and displacement (from a LVDT) data were recorded at a 10 Hz recording rate (Figure 3).

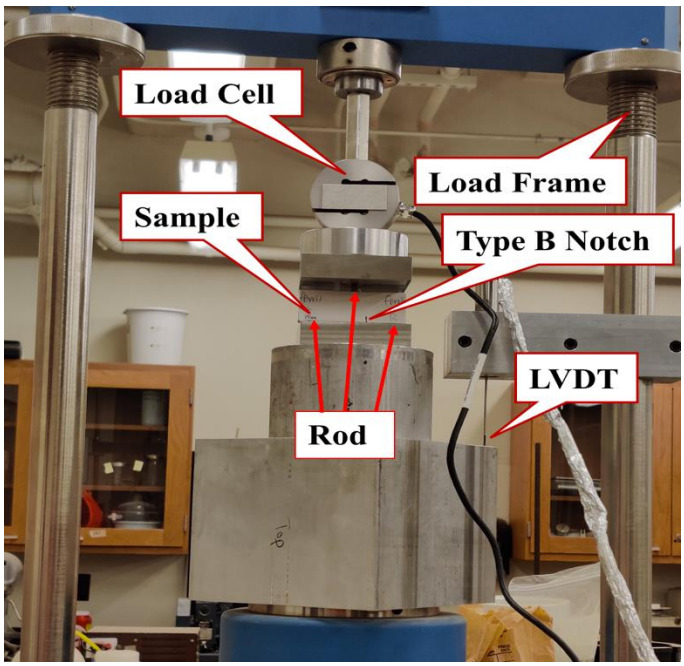

Fig. 3. 3PB testing setup with a type B sample being loaded

2.3. Fracture Roughness

After a sample failed, one of the fracture surfaces was scanned using laser profilometry to measure the surface roughness. A Keyence LK-G152 Laser (650 nm

wavelength, 120 um spot size) was fixed to a rail. The sample was mounted on coupled orthogonal translation stages (Newport MTM250PP1) and controlled by a motion controller (Newport Universal Motion Controller ESP 300) to enable measurements of asperity height over a 2D area (10 mm by 20 mm), in increments of 0.1 mm.

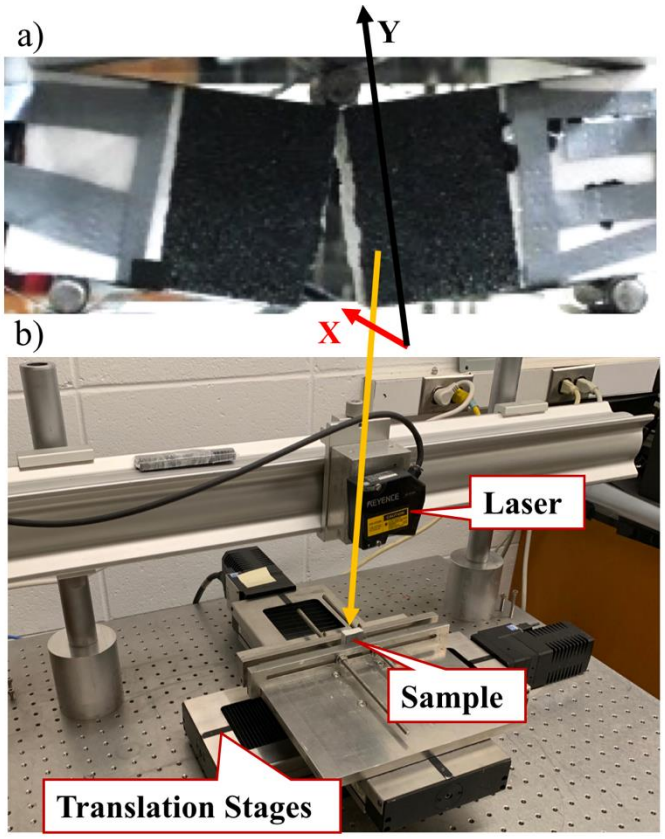

Fig. 4. Surface roughness measurement setup: (a) failed type C sample and coordinates for the asperity data; (b) laser profilometer setup with a piece of the fracture surface facing up

3. RESULTS

3.1. Peak Load

Though H type and HT type samples are both arrester with the same bedding layer orientation, the difference in the orientation of the in-plane mineral fabric resulted in different failure loads (Figures 5, 6, 7). Thus both the bedding layer and in-layer mineral fabric orientations must be considered when interpreting the resistance to fracturing. Maximum peak loads were observed (Figures 5, 6, 7) when both the bedding layers and mineral fabric orientations were perpendicular to the fracture plane (H), while minimum peak loads occurred when both the bedding layers and the mineral fabric orientations were parallel to the fracture plane (VT) for cases where fractures were initiated from the tip of the notch. For a given sample type (H, HT or VT), as the notch moved away from the center, the mode II loading increased, which resulted in an increase in the peak failure load (by 20% with notch 19.05 mm away from the center for sample H) (Figures 5, 6, 7). The peak load was repeatable within 10% error and the measured fracture path angles (see Section 3.2) were within 2 degrees error.

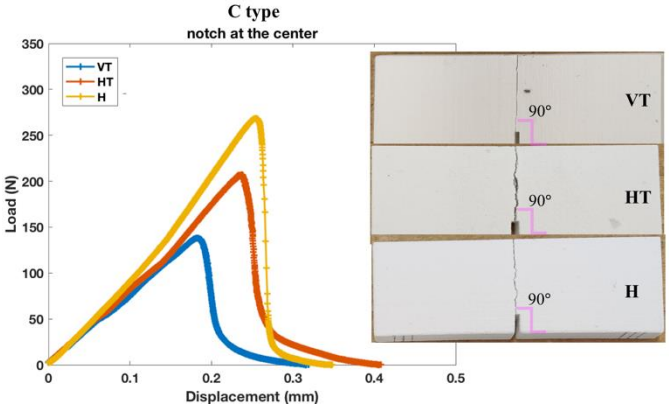

Fig. 5. Load displacement curves and fracture paths for Mode I loading (type C) are shown, together with a group of representative samples.

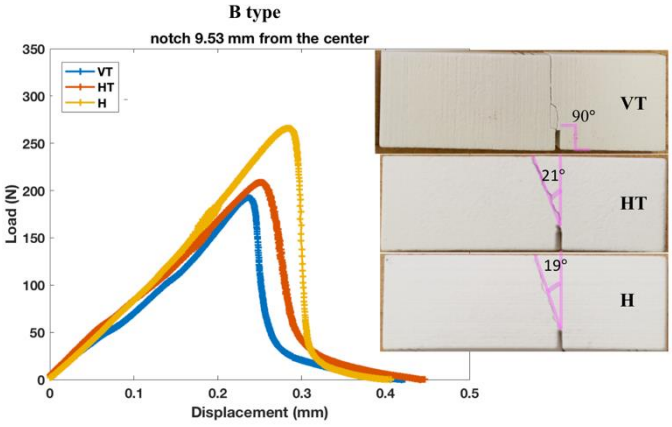

Fig. 6. Load displacement curves and fracture paths for mixed Mode I and II loading (type B) are shown, together with a group of representative samples. Each sample type was tested more than 3 times.

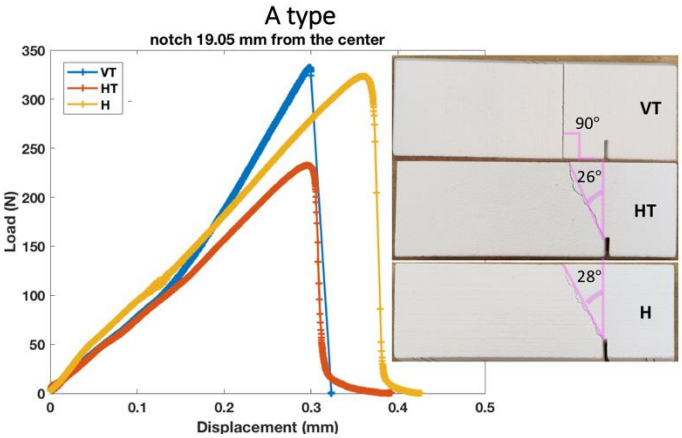

Fig. 7. Load displacement curves and fracture paths for mixed mode Mode I and II loading (type A) are shown, together with a group of representative samples. Each sample type was tested more than 3 times, the peak load was repeatable within 10%

error and the fracture path angle measurements was within 2 degrees error.

3.2. *Fracture Path*

Figures 5, 6 and 7 contain digital images of the samples post failure. The crack path and length, as a function of notch location, are the same for samples with the same bedding layer orientation (H & HT). Here, the orientation of the mineral fabric did not affect the crack path. The fractures, for both H and HT samples, initiated from the top of the tip of the notch and propagated towards the center of the sample where the load was applied. As the notch moved away from the center, the angle between the fracture path and the loading direction increased (Figure 5, 6, 7). However, for VT samples, the fracture path tended to be parallel to the loading direction and parallel to the layering regardless of notch location (Figures 5, 6, 7); also when the notch was located the farthest from the center, the fracture did not initiate from the tip of the notch (Figure 7). The competition between mode I and mode II during fracturing in this strongly layered material produced very different fracturing paths.

3.3. *Fracture Roughness*

The factors that determine whether an induced tensile fracture is smooth or rough, or whether it exhibits direction-dependent roughness depend on the relative resistance to failure among the rock constituents and structural features. Both the layering and the mineral fabric can cause a fracture to wander or deviate from a straight path, creating roughness along the fracture surfaces.

Figure 8 shows the scanned fracture surfaces formed in the three types of samples tested. When both the bedding layers and mineral fabric orientations were perpendicular to the loading, the fracture surface roughness was observed to be isotropic (H sample), while in all other cases a strong anisotropy was observed, with the smoother direction being parallel to the direction of the mineral fabric (VT and HT samples).

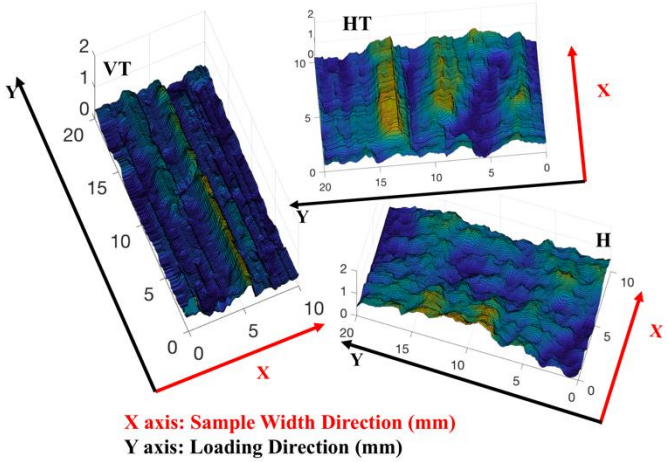

Fig. 8. 3D view of the surface roughness of samples with different bedding layers and mineral growth orientation directions (type C).

Whether the fracture roughness of a sample was isotropic or anisotropic was not determined by the notch location (Table 1). Here, we corrected the surface roughness maps for arbitrary rotations associated with mounting the sample in the laser profilometer system. Micro-slope angles (Jiang et al., 2020) were calculated from gradients of the asperity map in both the x and y directions (Figure 8). Table 1 shows the full width half maximum (FWHM) values of the micro-slope angles from the distribution taken in x and y directions from a group of representative samples. A ±15% deviation in FWHM values were observed from the samples of the same type and with the same notch location. Based on this, the FWHM are essentially the same for all of the different notch locations for a given sample type.

Table. 1. Full width half maximum (FWHM) values of the micro slope distributions in both X and Y directions from the fracture surfaces formed with different bedding layer and mineral growth directions (sample type VT, HT, H) and different notch locations (type A, B, C).

	X axis			Y axis		
	C	B	A	C	B	A
VT	5°	8°	6°	7°	8°	5°
HT	9°	13°	15°	29°	42°	30°
H	27°	31°	35°	23°	31°	27°

4. SUMMARY

3D printed rock is instrumental in unraveling the complexity and heterogeneity observed in fracture formation in natural rocks. It enables directional control of the in-layer mineral fabric, in layered samples, and in a repeatable manner.

Compared to the results from previous work (Jiang et al., 2019; Jiang et al., 2020) that found that differences in failure load and fracture roughness for layered rock are affected by both the layer and mineral fabric orientations, this work has discovered that the fracture path is influenced by the bedding and mineral fabric directions, when mode II loading is introduced. However, the surface roughness attributes (isotropy/anisotropy) are similar to those found from pure Mode I loading.

The results discussed suggest that detailed mineralogical studies of mineral texture/fabric in laboratory samples is important to unravel failure strength, surface roughness, and how fractures propagate in layered geological media. With this information, we have the potential to predict preferential flow paths in anisotropic fractures based on microscopic inspection of mineral texture orientation relative to layering, and the mode of failure, which are

vital to induced fracturing, geothermal and CO_2 capture applications.

5. ACKNOWLEDGMENT

We acknowledge the 3D X-Ray Microscope Facility in the Department of Physics for the images shown in this presentation, which were acquired on a Zeiss Xradia 510 Versa 3D X-ray Microscope that was supported by the EVPRP Major Multi-User Equipment Program 2017 at Purdue University. This material is also based upon work supported by the U.S. Department of Energy, Office of Science, Office of Basic Energy Sciences, Geosciences Research Program under Award Number (DE-FG02-09ER16022). Sandia National Laboratories is a multi-mission laboratory managed and operated by National Technology and Engineering Solutions of Sandia, LLC, a wholly owned subsidiary of Honeywell International, Inc., for the U.S. Department of Energy's National Nuclear Security Administration under contract DE-NA0003525. Any subjective views or opinions that might be expressed in the abstract do not necessarily represent the views of the U.S. Department of Energy or the United States Government.

REFERENCES

1. Jones, L. E. A. & Wang, H. F. Ultrasonic velocities in cretaceous shales from the Williston basin. *Geophysics* 46, 288–297 (1981).
2. Jiang, L., Yoon, H., Bobet, A., & Pyrak-Nolte, L. J. (2019, August 28). Effect of Mineral Orientation on Roughness and Toughness of Mode I Fractures. *American Rock Mechanics Association*.
3. Jiang, L., Yoon, H., Bobet, A. et al. Mineral Fabric as a Hidden Variable in Fracture Formation in Layered Media. *Sci Rep* 10, 2260 (2020).
4. Kong, L., Ostadhassan, M., Li, M. & Tamimi, N. Can 3-d printed gypsum samples replicate natural rocks? an experimental study. *Rock Mech. Rock Eng.*(2018).
5. Nejati, M., et al. "On the directional dependency of Mode I fracture toughness in anisotropic rocks." Theoretical and Applied Fracture Mechanics 107 (2020): 102494.
6. Sayers, C. M. Seismic anisotropy of shales. *Geophysical Prospecting* 53(2005).
7. Vernik, L. & Nur, A. Ultrasonic velocity and anisotropy of hydrocarbon source rock. *Geophysics* 57(1992).
8. Wenk, H.-R., Lonardelli, I., Herman, F., Nihei, K. T. & Nakagawa, S. Preferred orientation and elastic anisotropy of illite-rich shale. *Geophysics* 72, E69–E75 (2007).
9. Yu, M., Wei, C., Niu, L., Li, S. & Yu, Y. Calculation for tensile strength and fracture toughness of granite with three kinds of grain sizes using three-point-bending tests. *PLoS ONE* 13, 20(2018)
10. Hornby, B. E. , L. M. Schwartz, and J. A. Hudson, 1994, Anisotropic effective-medium modeling of the elastic properties of shales, Geophysics, vol. 59, Issue 10, p. 1492-1632.
11. Sayers, C.M., 1994, The elastic anisotrophy of shales, Journal of Geophysical Research: Solid Earth, vol. 99, Issue B1, p. 767-774, https://doi.org/10.1029/93JB02579